Fault Diagnosis of MEMS Lateral Comb Resonators Using Multiple-Model Adaptive Estimators

Afshin Izadian and Parviz Famouri, *Senior Member, IEEE*

***Abstract*—In this brief a fault diagnostic unit is developed for microelectromechanical systems (MEMS) by means of multiple model adaptive estimation technique. Fault modeling tools such as contamination and reliability analysis of microelectromechanical layout enabled interpretation of microsystems behavior by evaluating their structural variations and modeling them in form of electric circuits. This technique cannot directly diagnose the faults during operation of microsystems. However, these fault-representing models can be used in multiple model adaptive estimation technique to form fault diagnosis units. Here, fault-representing systems are modeled by Kalman filters in real-time applications and are used to evaluate the fault in microsystems. MEMS lateral comb resonators are fabricated to experimentally demonstrate the fault diagnosis performance in multiple model adaptive estimation technique.**

***Index Terms*—Adaptive estimators, fault diagnosis, Kalman filtering, lateral comb resonators (LCRs).**

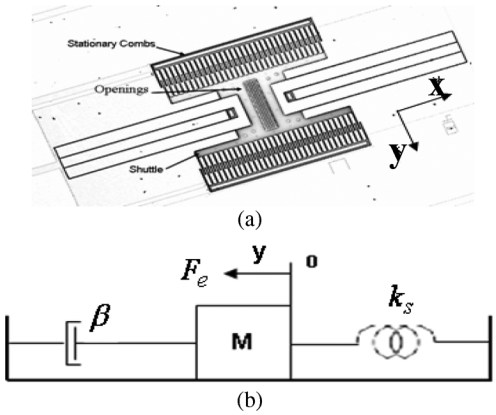

Fig. 1. (a) Lateral comb resonator designed by WVU. (b) Mass-spring-damper, schematic model of LCR.

I. Introduction

MICROELECTROMECHANICAL SYSTEMS (MEMS) are becoming the most important part of many advanced applications ranging from satellite stabilizers to commercial accelerometers. In simplest form, a MEMS lateral comb resonator (LCR) consists of two sets of fixed combs on both sides of a moving stage. The shuttle (moving part) has a comb-shape structure with fingers placed in the space between those on the fixed structure [see Fig. 1(a)]. The shuttle is suspended on two sets of springs and can be laterally displaced by electrostatic force generated between comb fingers. Fabrication process of MEMS involves several steps which might introduce parameter uncertainties in microsystems and cause high infant mortality rate. Different techniques are developed to measure the infant mortality rate in microfabrication processes [26]. Identifying the origins of these variations can be facilitated by deploying model matching techniques which allocate a predefined model to an operating system instantly. Therefore, a mechanism to model fault representing system is required.

Manuscript received July 15, 2008; revised March 24, 2009 and September 26, 2009; accepted October 20, 2009. Manuscript received in final form November 09, 2009. First published February 05, 2010; current version published August 25, 2010. Recommended by Associate Editor R. Rajamani. This work was supported in part by NASA and by NSF.

A. Izadian was with the Department of Chemistry and Biochemistry, University of California at Los Angeles, Los Angeles, CA 90095 USA. He is now with Purdue School of Engineering and Technology, IUPUI, Indianapolis, IN 46202 USA (e-mail: aizadian@iupui.edu).

P. Famouri is with the Lane Department of Computer Science and Electrical Engineering, West Virginia University, Morgantown, WV 26506 USA (e-mail: pfamouri@wvu.edu).

Color versions of one or more of the figures in this brief are available online at http://ieeexplore.ieee.org.

Digital Object Identifier 10.1109/TCST.2009.2036717

Faults can be modeled in MEMS by utilizing a recently developed tool such as contamination and reliability analysis of microelectromechanical layout (CARAMEL), which interprets system structural variations by finite element techniques and computes lumped parameters to represent the fault model in electric circuits [1], [2]. In this technique, suitable models containing different fault possibilities can be obtained. Kolpekwar *et al.* have modeled up to 4000 types of structural defects by CARAMEL [1]. CARAMEL can model an individual system to represent a particular type of fault offline; hence, a diagnostics technique is required for in-operation devices to detect the type of fault. In addition, defects such as change of operating environment, e.g., satellites, fluid control devices, and micro-pumps, in which microsystem is under influence of radiation, rapid environmental changes, and noise [3], cannot be modeled by CARAMEL.

Complicated structure of MEMS devices like gyroscopes and micromirrors can be simplified into several basic elements such as parallel plate actuators and lateral comb resonators. Monitoring technique for a basic element such as a LCR will define the guideline for diagnostics of more complicated devices. In this brief, a LCR is used for fault diagnostic studies. Lateral comb resonators can be modeled in a second-order mass-spring-damper system. In order to take the parameter variations originated from manufacturing, in-operation wearing of the parts and fault into account, the coefficients of microsystems are considered time-dependent values. Structural variations can also be modeled as a shift in the values of these parameters. Loss of vacuum, severe shocks, and manufacturing defects are common types of fault in microsystems, which are modeled by damping coefficient and spring constant variations. Severe structural damages might impair the device and cause failure which result in a nonworking device. In fault diagnostics and supervisory monitoring of MEMS, some specific parameter varia-

tions are of particular interest. Therefore, as defined, each fault case might cover different parameter variations and result in a unique subsystem representing that fault. Number of these subsystems can be arbitrarily set according to the application and system operating requirements. Several techniques are used to evaluate these models and diagnose the fault in the system.

In this brief, Kalman filters are utilized to model the MEMS devices and to accurately factor in the system and measurement noise resulted from the hybrid optical measurement technique. The displacement of MEMS is measured by a laser beam in a propagation, collection and recovery loop. Multiple-model adaptive estimators are applied in fault diagnosis of lateral comb resonators and their simulations are experimentally verified in test of fabricated devices. The effect of noise in decision-making process is studied for over and underestimated noise in LCR systems.

II. Lateral Comb Resonator and Modeling

A. MEMS

Recently, MEMS became an important part of very precise applications because of their low cost and high accuracy of operation. They are also available for commercial use in different forms and applications. A simple form of an actuator is a LCR, which is used in many complicated devices such as gyroscopes. LCR structure contains a moving stage also known as shuttle, stationary combs and suspension springs on both sides along the Y-axis [see Fig. 1(a)]. The LCR can be modeled as a mass spring damper [see Fig. 1(b)] in a second-order linear differential equation. The electrostatic force is generated by applying two identical dc voltages onto the stationary combs at both sides of the LCR. The ideal electrostatic force depicted in (1) is a function of applied voltages and geometry of the device; however, there are many other phenomena that affect the force values that are not considered in electrostatic force equation [3]. The ideal force is

$$F_e = -4n\varepsilon\frac{t}{g}(V_b.V_s) \tag{1}$$

where F_e is the electrostatic force, n is the number of fingers in one side, ε is the permittivity of air, t is the length of a finger, g is the gap between fingers, V_b, V_s are applied stator and shuttle's body voltages, respectively. A simple mass-spring-damper model of the system can be written as

$$F_e = m\ddot{y} + \beta\dot{y} + 2k_s y + F_d \tag{2}$$

where m is the mass of the center comb (shuttle), y is the displacement, k_s is the spring constant of one side, β is the damping coefficient, F_d is the force due to load. In many microstructure applications such as connecting a beam to rotating gears, the load can be applied directly to the shuttle.

As mentioned earlier, the device parameters are affected by manufacturing processes, operating and environmental conditions. Under these conditions, the model containing uncertainties can be expressed as

$$\hat{F}_e = \hat{m}\ddot{y} + \hat{\beta}\dot{y} + 2\hat{k}_s y + \hat{F}_d \tag{3}$$

where $\hat{(\ )}$ denotes the uncertain values of parameters. The fact is that the desired system should operate similar to (2) whereas the manufactured device which behaves differently and is represented by (3). More details on model parameter uncertainties, control application and displacement monitoring technique, which is also used in this brief, can be found in [5]–[21]. The state space governing equation of a MEMS LCR considering uncertain values can be represented as

$$\begin{cases} \dot{x}_1 = x_2 \\ \dot{x}_2 = \frac{1}{\hat{m}}(-2\hat{k}_s x_1 - \hat{\beta}x_2) + \frac{\hat{F}_e - \hat{F}_d}{\hat{m}}. \end{cases} \tag{4}$$

The second-order state space equations describe dynamical behavior of microsystem in different conditions, i.e., change of mass, spring constant, and damping coefficients can generate entirely different sets of equations and result in various equilibrium points.

B. Optical Monitoring Technique

Application of an optical method for measuring the displacement of the shuttle location is described in this section. Several researchers have used optical monitoring technique in measuring the displacement [30]–[32]. Displacement of the shuttle can also be measured by through wafer optical monitoring technique [28] to validate the position of the shuttle simultaneously. The through wafer optical displacement-monitoring system contains an infrared waveguide of wavelength 1310 nm emitted from a laser diode. Two bulk lenses focus the beam on the device from the bottom side, which is polished by a 0.1-μm polisher in order to reduce the beam scattering and ray loss.

The laser emitted out of the grating structure is collected and directed to the detector through a multimode fiber optic detector probe that houses a single-mode detector fiber. As the shuttle "center comb" moves, its body cuts the laser beam through the openings and produces pulses. The detector then experiences the intensity changes of the beam due to the shuttle displacement; therefore, the output voltage of the detector contains the grating-encoded displacement information of LCR. The alignment of the output laser beam and the detector fiber optic coming out of the openings on the device is the critical point for obtaining the highest possible signal-to-noise ratio (SNR). The Gaussian distribution of the laser beam allows the system to concentrate on the openings and reduce the spot size on the device [7]. A schematic of the through wafer optical monitoring technique is shown in Fig. 2. The collected optical data is then transferred to the data recovery algorithm that determines the instantaneous displacement of the shuttle [5], [6]. The research on the integration of an *in-situ* structure of the laser beam emitter and collector is in progress [29]. Therefore, an advanced integrated optical displacement monitoring technique seems practical.

III. Fault in LCRs

As illustrated in Section II, a second-order mass-spring-damper system is used to model lateral comb resonators. This brief investigates the parametric uncertainties and those kinds

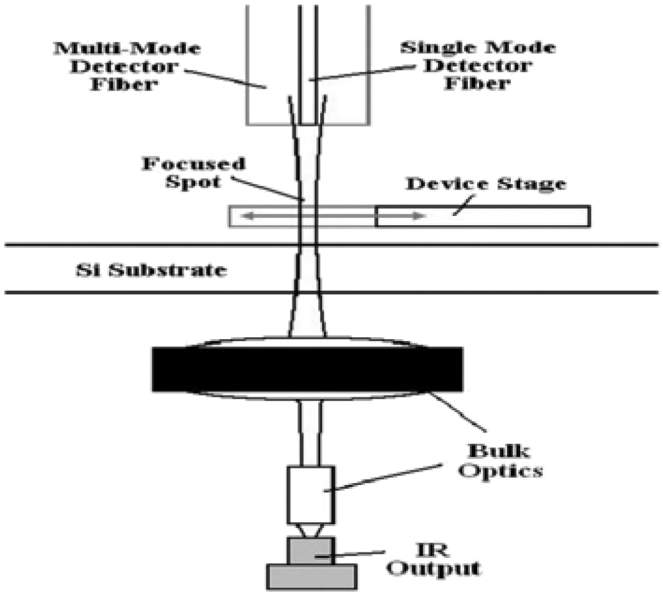

Fig. 2. Optical through wafer monitoring system.

of structural uncertainties that can be modeled as linear parameter variation.

Fault in microsystems can be originated from local defects, parameter tolerances, design problems, operation, and/or system level defects [4]. Faults might happen by breaking different parts of the device such as suspension springs or fingers (in LCR). In any of these cases, asymmetries result in behavioral changes and unwanted deviations from the desired output.

In open-to-air applications, there is a chance that dust and other particles fall on the structure of the device, which may cause a change of mass of the shuttle. In addition, the silicon made structures absorb humidity of air that result in change of mechanical properties of suspension springs. Larger size conductive particles on areas between two fingers on shuttle and fixed structures might cause a short circuit in the device, join the parts together and result in a failure. For devices operating in vacuum conditions, any damage in the container might result in the loss of vacuum and consequently change of viscosity.

In physical systems, fault can be defined when the variation of a particular parameter or a set of parameters exceed a predefined threshold, e.g., when the mass or spring constant stiffness exceed a threshold. Several individual parameters or their combinations can be monitored in various models to determine the amplitude of the fault in the system. Monitoring the behavior of a system respect to some specific parameters and thresholds require multiple model developments where each is tuned at some desired threshold level to specifically diagnose the level of changes in the system. Therefore, not all levels of parameter variations are considered in models.

A fault scenario is developed in Section V that covers most common types of parameter variations. MEMS LCRs are also fabricated with different parameters to experimentally examine the diagnostic capabilities of multiple-model adaptive estimation technique.

IV. Fault Diagnosis Theory Development

A. Kalman Filter Design for LCRs

Consider the steady-state Kalman filter model of an LCR associated with different types of fault conditions denoted by subscript k as

$$\begin{aligned} x_k(t_i) &= \Phi_k x_x(t_{i-1}) + \Gamma_k u(t_{i-1}) + G_k w_k(t_i) \\ z_k(t_i) &= H_k x_k(t_i) + v_k(t_i) \end{aligned} \tag{5}$$

where x_k is the Kalman filter model's state-space variables (displacement and speed of the shuttle), Φ_k is the system matrix, Γ_k is the input matrix, u is the input vector, G_k is the Kalman filter model's input noise matrix, w_k is the input noise with zero mean and variance of

$$E\left\{w_k(t_i)w_k^T(t_j)\right\} = \begin{cases} Q_k, & t_i = t_j \\ 0, & t_i \neq t_j \end{cases} \tag{6}$$

z_k is the measurement vector (displacement and speed of the shuttle), H_k is the output matrix, $v_k(t_i)$ is the output measurement noise, independent from w_k, with zero mean value as

$$E\left\{v_k(t_i)v_k^T(t_j)\right\} = \begin{cases} R_k, & t_i = t_j \\ 0, & t_i \neq t_j. \end{cases} \tag{7}$$

Kalman filter model representation of a system is

$$\hat{x}_k(t_i) = \Phi_k \hat{x}_x(t_{i-1}) + \Gamma_k u(t_{i-1}) + K_e\left(y_k(t_i) - H_k \hat{x}_k(t_i)\right) \tag{8}$$

where $\hat{x}_k$ is the estimation of state space variable, y_k is the actual output expected from the model, and K_e is the Kalman filter gain recursively obtained through the following procedure:

$$K_e(n) = \Phi_k P(n) H_k^T \left[R + H_k P(n) H_k^T\right]^{-1} \text{ for } n = 1, 2, \ldots \tag{9}$$

where P is the covariance matrix updated by

$$\begin{aligned} P(n+1) = {} & G_k Q G_k^T + \Phi_k P(n) \Phi_k^T \\ & - \Phi_k P(n) H_k \left[R + H_k P(n) H_k^T\right]^{-1} H_k P(n) \Phi_k^T. \end{aligned} \tag{10}$$

The covariance matrix P updates the Kalman gains recursively. The residual signal is defined as the difference between the output of the Kalman filter model and that of the actual operating system. For each of the models there is a residual signal computed instantaneously and used to compute conditional probability density functions. Residual signals are obtained as

$$r_k(t_i) = z(t_i) - H_k \hat{x}_k(t_i)). \tag{11}$$

B. Multiple-Model Adaptive Estimation Technique

A hypothesis-testing algorithm continuously monitors the residual signal variations. If the output of any of Kalman filters matches the output of the system and makes the mean value

of residual signal zero, then the covariance matrix can be computed by [17], [22]

$$\psi_k = H_k P_k H_k^T. \tag{12}$$

Conditional probability density functions of the kth Kalman filter model considering the history of measurement $Z(t_{i-1}) = [z^T(t_1), \ldots, z^T(t_{i-1})]$ is expressed as [22]

$$f_{z(t_i)|h,Z(t_{i-1})}(z_i|h_k, Z_{i-1}) = \beta_k \exp\{\bullet\} \tag{13}$$

with

$$\beta_k = \frac{1}{(2\pi)^{l/2}|\psi_k|^{l/2}} \tag{14}$$

and

$$\{\bullet\} = \left\{-\frac{1}{2} r_k^T(t_i)\psi_k^{-1} r_k(t_i)\right\} \tag{15}$$

where r_k is the residual signal as defined in (11). The conditional probability evaluation of the kth system is defined as

$$p_k(t_i) = P\{h = h_k | Z(t_i) = Z_i\}. \tag{16}$$

This value can also be computed by [22]

$$p_k(t_i) = \frac{f_{z(t_i)|h,Z(t_{i-1})}(z_i|h_k, Z_{i-1}).p_k(t_{i-1})}{\sum_{j=1}^{K} f_{z(t_i)|h,Z(t_{i-1})}(z_i|h_j, Z_{i-1}).p_j(t_{i-1})}. \tag{17}$$

The conditional probability density functions require *a priori* samples to compute the current values and are normalized over a complete sum of the conditional probabilities of all systems [9]. The largest conditional probability among all can be used as an indicator of fault in the systems (note that each fault-representing system should be modeled separately). In addition, they can associate weight to the outputs of the systems to define weighted output for each fault-model. In some applications, probabilities change rapidly and make the output of the system unpredictable then the output should be compared with a threshold. The system contains a zero mean white noise with $Q = 1e-6$, $R = 1e-6$ covariance values in the measurement signal and system, respectively.

V. Diagnostic Performance Evaluation

A. Fault Diagnosis

To simulate the fault diagnosis technique, a sequence of events concerning the main parameter variations is used as fault scenario. Majority of fault diagnosis techniques would latch the state of the recognized fault; however, to investigate the capability of the MMAE and Kalman filter, identical start and end health conditions are included in the fault scenario. Examples of typical parameter variations resembling the actual fault can be identified in the following steps:

1) health operation for 2 k samples;
2) +5% mass variation for 1 k samples;
3) +10% mass variation for 1 k samples;

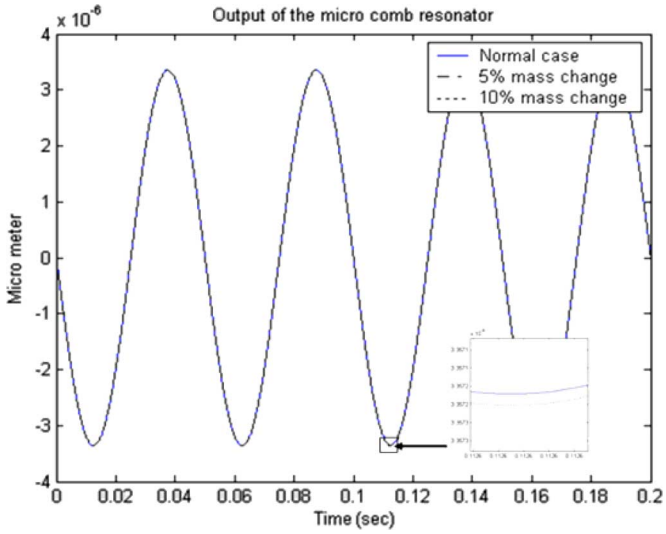

Fig. 3. Mass change effects on the system output displacement. All the outputs are very close since the influence of mass variation is negligible.

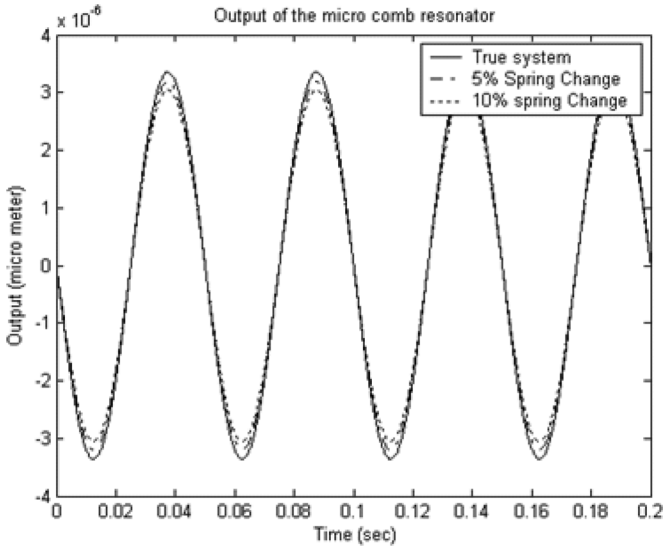

Fig. 4. Output displacement of the system in case of the spring constant change to 5% and 10%.

4) +5% spring constant variation for 1 k samples;
5) +10% spring constant variation for 1 k samples;
6) +30% change in damping coefficient for 1 k samples;
7) return to normal condition after 2 k samples.

These series of events occur consecutively and cover common types of variations that microsystems might undergo during their operation. The displacement variation in case of +5% and +10% change of the mass of LCR are shown in Fig. 3.

The displacement resulted from the spring constant variations are shown in Fig. 4. Any change in spring constant values cause higher displacement variations and stronger residual signals.

Damping coefficient variations cause a delay from the original waveform. Fig. 5 shows the phase shift resulted by a 30% change of damping coefficient and completely matches step 6 of the fault scenario.

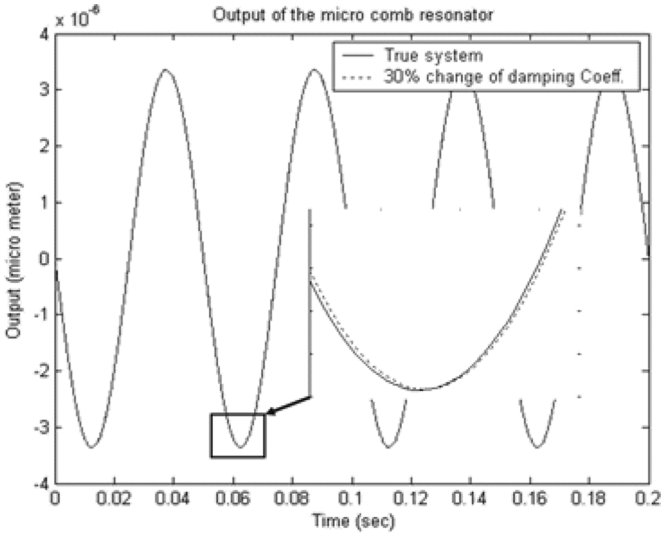

Fig. 5. Effect of the spring constant change on the LCR's output, 30% change from the true system output.

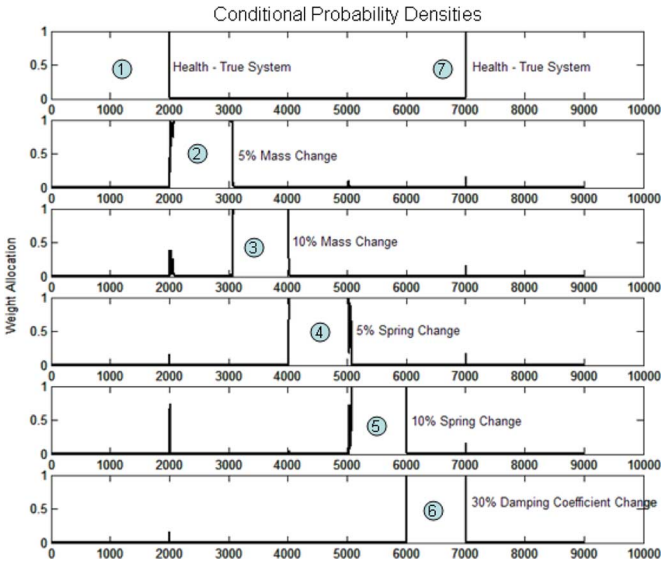

Fig. 6. Conditional probability density function outputs over different cases of the fault scenario. Higher output values show the validity of the case and as a result the diagnosis of the fault. Numbers 1–7 show different steps of fault scenario.

The noise content in microsystem has significant effect on the conditional probability functions. The effect of noise in fault diagnosis is studied in two cases of noise under and overestimation in Kalman filter designs. Considering normal noise content in microsystem and its environment, Kalman gains are computed for each of these models.

Applying probability density functions on fault scenario designates a weight between 0 and 1 to each system's output in each time instant. Higher probability numbers indicate validity of that particular system in that sample. Fig. 6 shows the weight allocation computed by probability density functions in evaluation of the residual signal in case of normal noise content in microsystems. As Fig. 6 shows, the highest weight is allocated to a proper system (numbered according to the fault scenario) which accurately follows the scenario.

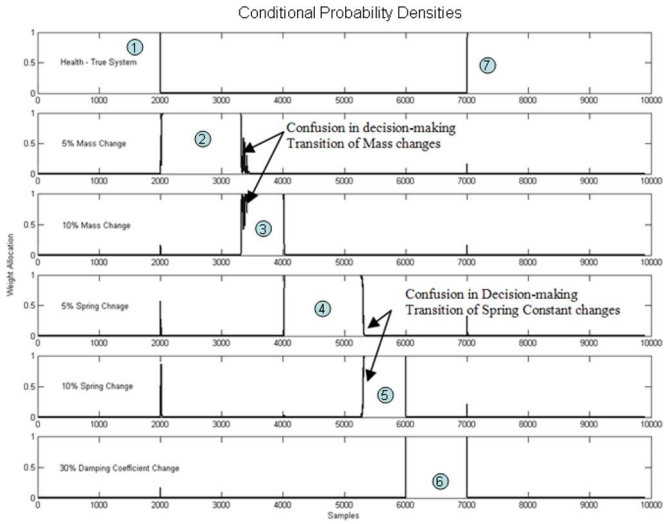

Fig. 7. Conditional probability function outputs over different cases of the fault scenario in a 35% noise overestimation. Higher output values show the validity of the case and as a result the diagnosis of the fault.

As Fig. 6 shows, a quick transition is observed among steps. The MMAE fault diagnostic unit accurately identifies the faults as designed in the scenario.

In case the noise is overestimated from which actually existed in the system for Kalman gain computations, the fault diagnostic unit identifies the faults of different kind rapidly, i.e., the transition from mass change to spring constant is rapid. However, in the same category of parameter variations, the noise results in a delay in fault recognition (e.g., from 5% to 10% of mass variations), shown in Fig. 7. A 35% noise overestimation influences the transitions between 5% and 10% change of mass and spring constants individually, but still provides a quick transition from mass to spring constant variations. As the figure shows, delays in transitions from steps 2 to 3 and steps 4 to 5 were observed. Existence of noise masks small parameter variations and reduces the system's sensitivity which is required in high performance fault diagnosis system.

If the noise content in the system is underestimated from which actually exist in the system for Kalman gain calculations, the fault diagnostics results in inaccurate and random transitions among fault scenario steps, e.g., in transitions from steps 2 to 3, steps 3 to 4, and 4 to 5. Fig. 8 shows the noise underestimation results and its consequences on the decision-making process.

In a situation that the output of the actual system is between the outputs of two of the representative models (e.g., between 5% and 10% spring constant variations) the probability density of these models will rise to higher number (than zero) weighing more toward the closer subsystem to the actual system. In that case, an indicator would trigger the threshold mechanism and an appropriate fault code would be issued.

B. Experimental Results

Scheduling a precisely adjusted parameter variation in MEMS is possible in simulations but it is difficult to do the same task during the operation of one device. As mentioned earlier, fault conditions if defined in form of the parameter variation can be arbitrarily set to meet the system monitoring

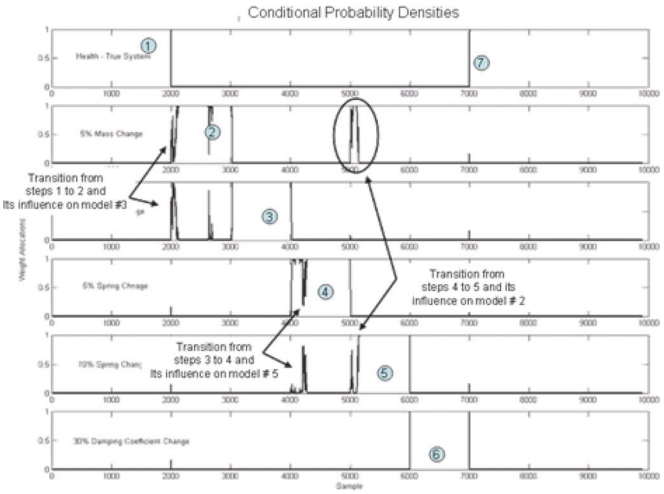

Fig. 8. Conditional probability function outputs over different cases of the fault scenario in case of 40% noise underestimation. Higher output values show the validity of the case and as a result the diagnosis of the fault in that.

TABLE I
ESTIMATED PARAMETERS OF TWO FABRICATED SYSTEM

	Mass	K_s	Beta
System #1	2.3856e-10	0.0193	7.563e-7
System #2	2.2429e-10	0.0448	1.385e-6

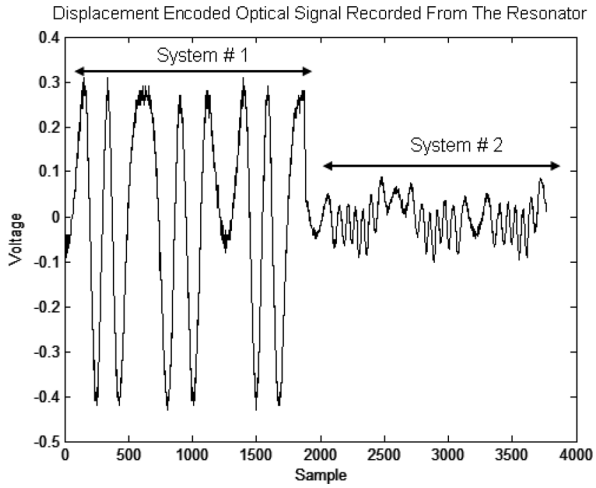

Fig. 9. Optical grating encoded displacement signals.

needs. In simulations, the performance of the MMAE was illustrated. To experimentally demonstrate the effectiveness of the diagnostics approach of this brief, two healthy MEMS devices with known and different parameters were selected. The knowledge of the parameter values is not necessary for actual implementations and is needed to set the parameter variations to define the fault during the operation. To design an accurate point of fault and evaluate the fault diagnosis technique performance, these devices were excited with the same input voltage. Their output displacement signals were recorded separately and joined together to obtain one waveform with a fault scheduled in it. The amount of parameter variation from device #1 to device #2 is defined to resemble a fault occurrence in the system. In practice, MEMS devices are being monitored individually. The resulted waveform (with fault) was fed to the algorithm to evaluate the fault diagnosis performance.

Fabrication of MEMS devices require several chemical reactions and layer depositions. Some of these steps can be controlled accurately. Table I shows the resulted parameters of two MEMS microcomb resonators fabricated in the same process [10]. To accurately select MEMS devices, their parameters were identified through genetic algorithm and curve fitting [10]. As Table I shows, mass contents of two devices are similar. The spring constant of two devices however were intentionally designed to be different, which required different geometries in MEMS. Damping coefficient is a function of several parameters among them the interface material density, and size and geometry of the moving plates that squeeze the interface material. These dependencies resulted in a damping coefficient variation in two fabricated devices. In reality, the damping coefficients vary significantly during the operation of the device since the fault condition can be as severe as loss of vacuum condition. Small variations in damping coefficient of an open-to-air device can mainly occur as a result of the temperature and humidity variations. However, the fault diagnosis technique is sensitive enough to identify these variations (as shown in fault simulations). The importance of the experiment with significant spring constant variation is to define a single fault dominating model of the device and to evaluate the diagnosis capabilities of the multiple model adaptive estimation technique. Similar goals can be achieved in devices with a set of parameters varying at the same time depend upon the application. Desired parameters and their threshold can also be set by CARAMEL [1], [2].

In order to measure the displacement of the device, an optical through wafer displacement monitoring technique was utilized (Section II-B). The displacement encoded optical waveforms of two devices are shown in Fig. 9. These devices were excited by a $10sin(4000\pi t)$ volt signal. To extract the displacement information of the shuttle from the optical signal, an auto-recovery unit was utilized. The extracted displacement signal is shown in Fig. 10. Interested readers can find more information on auto-recovery in [10].

Kalman filters were designed for devices with their gains shown in Table II. Covariance values of system and measurement noise were $Q = 0.00002$, $R = 0.00008$. Probability density values were initially set equally to 0.5. Both models are constantly being evaluated and their residual signals are processed in MMAE to identify the right model behavior. Fig. 11 shows the weight allocation (probability density values) and transition profile in the fault diagnostic unit. As this figure illustrates, higher probabilities are associated to system 1, making it valid for initial part of the simulation and all samples up to the 1886th (also marked as point 1 in Fig. 11).

There is small variation observed in the probability values because of the noise in the system. A quick transition in the probability values is observed when the fault occurs and the weight is shifted to validate the second system (point 2 in Fig. 10).

It can be observed from the simulation and experimental results that the system including Kalman filters and MMAE is capable of computing strong probability density functions to distinguish small and large parameter variations in physical systems. Associating these parameter variation to faults, one can

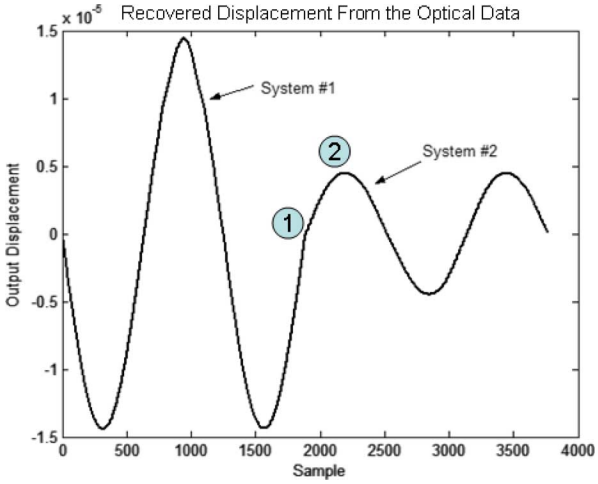

Fig. 10. Recovered displacement of LCRs. Point 1 shows the location of fault and point 2 shows the first peak of the second system output.

TABLE II
KALMAN FILTERING GAINS FOR SYSTEMS 1 AND 2

Ke_1	Ke_2
0.0013	0.0013
-1.5064	-3.5741

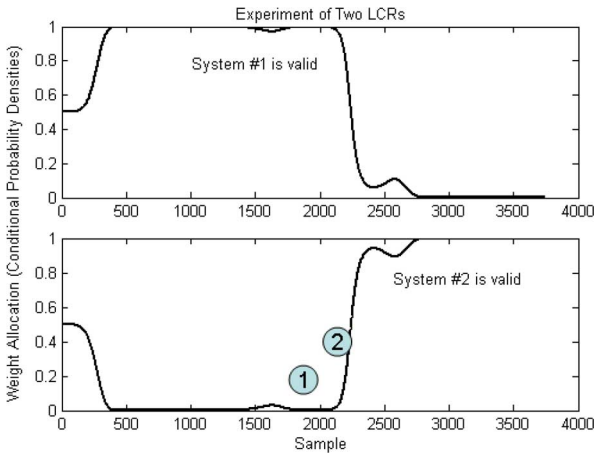

Fig. 11. Weight allocation and conditional probability densities. Switching performance from model of system #1 to model of system #2.

use this technique for fault diagnostics of predefined situations. This brief demonstrated the possibility of utilizing the MMAE technique in fault diagnosis of MEMS LCR devices.

VI. CONCLUSION

In this brief, a previously known multiple-model adaptive estimation technique was applied to the fault diagnosis of MEMS LCRs. Several systems with different parameters were designed to represent the fault conditions and form a fault scenario. Kalman filters were used in modeling of fault in microsystems considering various noise contents. The output displacement was used as the main fault indicator in the device. Successful application of MMAE in fault diagnosis of MEMS devices were experimentally demonstrated by means of fabricated LCRs. This brief successfully demonstrated the application of Kalman filters in modeling of slowly varying parameter systems and their usage in residual signal computations to be used in multiple model adaptive estimation technique for fault diagnostics.

ACKNOWLEDGMENT

The authors would like to thank Dr. L. Wang for her contribution in data acquisition and MEMS parameter identification.

REFERENCES

[1] A. Kolpekwar, C. Kellen, and R. D. Blanton, "MEMS fault model generation using CARAMEL," *J. Microelectromechan. Syst.*, vol. 8, no. 3, pp. 308–318, Sep. 1999.

[2] A. Kolpekwar and R. D. Blanton, "Development of MEMS testing methodology," in *Proc. IEEE Int. Test Conf.*, 1997, pp. 923–931.

[3] L. P. Schanwald, J. R. Schwank, J. J. Sniegowski, D. S. Walsh, N. F. Smith, K. A. Peterson, M. R. Shaneyfelt, P. S. Winokur, J. H. Smith, and B. L. Doyle, "Radiation effects on surface micro machined comb drives and microengine," *IEEE Trans. Nucl. Sci.*, vol. 45, no. 6, pp. 2789–2798, Dec. 1998.

[4] R. Rosing, A. Richardson, A. Dorey, and A. Peyton, "Fault Simulation for MEMS," in *Proc. Colloquium IEE Intell. Self-Validating Sensors (Ref. No. 1999/160)*, Jun. 21, 1999, pp. 7/1–7/6.

[5] A. Izadian and P. Famouri, "Reliability enhancement of micro comb resonators under fault conditions," *IEEE Trans. Control Syst. Technol.*, vol. 16, no. 4, pp. 726–734, Jul. 2008.

[6] L. Wang, J. M. Dawson, L. A. Hornak, P. Famouri, and R. Ghaffarian, "Real time transitional control of a MEMS comb resonator," *IEEE Trans. Aerosp. Electron.*, vol. 40, no. 2, pp. 575–576, Apr. 2004.

[7] J. M. Dawson, L. Wang, J. Chen, P. Famouri, and L. A. Hornak, "MEMS feedback control using through -wafer optical device monitoring," presented at the SPIE, Int. Soc. for Opt. Eng., Santa Clara, CA, Sep. 2000.

[8] J. M. Dawson, J. Chen, K. S. Brown, P. Famouri, and L. A. Hornak, "Through wafer optical probe characterization for micro electromechanically systems positional state monitoring and feedback control," *Opt. Eng.*, vol. 39, no. 12, pp. 3239–3246, Dec. 2000.

[9] S. Park, R. Horowitz, and C.-W. Tan, "Adaptive controller design of MEMS gyroscope," presented at the IEEE Intell. Transport. Syst. Conf., Oakland, CA, Aug. 2001.

[10] L. Wang, "Modeling and real-time feedback control of MEMS device" Ph.D. dissertation, Dept. Comput. Sci. Elect. Eng., West Virginia Univ., Morgantown, 2005. [Online]. Available: https://eidr.wvu.edu/etd/documentdata.eTD?documentid=3711

[11] A. M. Shkel, R. H. Horowitz, A. A. Seshia, S. Park, and R. T. Howe, "Dynamics and control of micromachined gyroscopes," in *Proc. Amer. Control Conf.*, San Diego, CA, Jun. 1999, pp. 2119–2124.

[12] R. Horowitz, P. Cheung, and R. T. Howe, "Position sensing and control of electrostatically driven polysilicon micro actuator," presented at the ASME Micromech. Syst. Symp. (ICE), San Francisco, CA, Nov. 1995.

[13] G. K. Fedder and R. T. Howe, "Multimode digital control of suspended polysilicon microstructure," *IEEE J. Microelectromechan. Syst.*, vol. 5, no. 4, pp. 283–297, Dec. 1996.

[14] W. T. Tang, M. G. Lim, and R. T. Howe, "Electrostatic comb drive levitation and control method," *IEEE J. Microelectromechan. Syst.*, vol. 1, no. 4, pp. 170–178, Dec. 1992.

[15] A. Izadian, L. A. Hornak, and P. Famouri, "Structure rotation and pull-in voltage control of MEMS lateral comb resonators under fault conditions," *IEEE Trans. Control Syst. Technol.*, vol. 17, no. 1, pp. 51–59, Jan. 2009.

[16] J. M. Dawson, J. Chen, K. S. Brown, P. Famouri, and L. A. Hornak, "Through wafer optical probe characterization for micro electromechanically systems positional state monitoring and feedback control," *Opt. Eng.*, vol. 39, no. 12, pp. 3239–3246, Dec. 2000.

[17] A. Izadian, P. Khayyer, and P. Famouri, "Fault diagnosis of time-varying parameter systems with application in MEMS LCRs," *IEEE Trans. Ind. Electron.*, vol. 56, no. 4, pp. 973–978, Apr. 2009.

[18] S. Bhansali, A. L. Zhang, R. B. Zmood, P. E. Jones, and D. K. Sood, "Prototype feedback-controlled bi-directional actuation system for MEMS applications," *J. Microelectromechan. Syst.*, vol. 9, no. 2, pp. 245–251, Jun. 2000.

[19] Y. Li and R. Horowitz, "Active suspension vibration control with dual stage actuators in hard disk drives," in *Proc. Amer. Control Conf.*, Arlington, VA, Jun. 2001, pp. 2786–2791.

[20] S. Pannu, C. Chang, R. S. Muller, and A. P. Pisano, "Closed-loop feedback control systems for improved tracking in magnetically actuated micro mirrors," in *Proc. IEEE/LEOS Int. Conf. Opt. MEMS*, Kauai, HI, Aug. 2000, pp. 107–108.

[21] P. D. Hanlon and P. S. Maybeck, "Multiple-model adaptive estimation using a residual correlation Kalman filter bank," *IEEE Trans. Aerosp. Electron. Syst.*, vol. 36, no. 2, pp. 393–406, Apr. 2000.

[22] S. B. Brown, C. Muhlstein, C. Chui, and C. Abnet, "Testing of MEMS material properties and stability," in *Proc. IEEE Readiness Technol. Conf.*, Aug. 1998, pp. 161–162.

[23] J. Tanha and R. Asgary, "An intelligent BIST mechanism for MEMS fault detection," in *Proc. Int. Conf. Perspective Technol. Methods MEMS Des. (MEMSTECH)*, May 2007, pp. 12–14.

[24] S. K. Tewksbury, "Challenges facing practical DFT for MEMS," in *Proc. IEEE Int. Defect Fault Toler. VLSI Syst.*, Oct. 2001, pp. 11–17.

[25] K. W. Alt, R. E. Yeats, C. P. Hutchinson, D. K. Low, M. Iwamoto, M. E. Adamski, R. L. Shimon, T. E. Shirly, M. Bonse, F. G. Kellert, and D. C. D'Avanzo, "Measurement of infant mortality rate in InGaP/GaAs heterojunction bipolar transistor technology," in *Proc. Reliab. Compound Semicond. (ROCS) Workshop*, Nov. 2006, pp. 117–127.

[26] X. Wu, J. Zhe, J. Wang, J. Cheng, V. Modi, and K. R. Farmer, "A generalized capacitance-based model for electrostatic micro-actuators," [Online]. Available: www.njit.edu/v2/MRC/mrcpdf/wuappliedphysicsletter_v6.pdf

[27] D. L. Konduparthi, "Optical detection of multiple faults on MEMS based linear comb resonator" M.S. thesis, Dept. Comput. Sci. Elect. Eng., West Virginia Univ., Morgantown, 2005. [Online]. Available: https://eidr.wvu.edu/etd/documentdata.eTD?documentid=4424

[28] W. McCormick, "Diffractive optical lens design for integrated monitoring of microelectromechanical lateral comb resonator," M.S. thesis, Dept. Comput. Sci. Elect. Eng., West Virginia Univ., Morgantown, 2004.

[29] N. A. Hall, M. Okandan, and F. L. Degertekin, "Surface and bulk-silicon-micromachined optical displacement sensor fabricated with the SwIFT-Lite ™ process," *J. Microelectromechan. Syst.*, vol. 15, no. 4, pp. 770–776, Aug. 2006.

[30] G. Zhou and F. S. Chau, "Grating-assisted optical microprobing of in-plane and out-of-plane displacements of microelectromechanical devices," *J. Microelectromechan. Syst.*, vol. 15, no. 2, pp. 388–395, Apr. 2006.

[31] U. Krishnamoorthy, R. H. Olsson, III, G. R. Bogart, M. S. Baker, D. W. Carr, T. P. Swiler, and P. J. Clews, "In-plane MEMS-based nano-g accelerometer with sub-wavelength optical resonant sensor," *J. Sensors Actuators A: Phys.*, vol. 145–146, pp. 283–290, Jul.–Aug. 2008.

[32] H. Ma, "Capacitive displacement sensing for the nanogate" M.S. thesis, Sch. Arch. Planning, Massachusetts Institute of Technology, Boston [Online]. Available: http://www.media.mit.edu/resenv/pubs/theses/HongMa-MSThesis.pdf